

# Inertio-elastic instability in Taylor-Couette flow of a model wormlike micellar system

Hadi Mohammadigoushki<sup>1</sup> and Susan J. Muller<sup>2\*</sup>

<sup>1</sup>Department of Chemical and Biomedical Engineering

Florida A&M University - Florida State University, College of Engineering, Florida 32310, United States

<sup>2</sup>Department of Chemical and Biomolecular Engineering

University of California, Berkeley, California 94720, United States

## Abstract

In this work, we use flow visualization and rheometry techniques to study the dynamics and evolution of secondary flows in a model wormlike micellar solution sheared between concentric cylinders, i.e., in a Taylor-Couette (TC) cell. The wormlike micellar solution studied in this work contains cetyltrimethylammonium bromide (CTAB) and sodium salicylate (NaSal). This system can be shear banding and highly elastic, non-shear banding and moderately elastic, or nearly Newtonian as the temperature is varied over a narrow range. The effect of elasticity on transitions and instabilities is probed by changing the temperature over a wide range of elasticity ( $El \ll 1$ ,  $El \approx 1$ , and  $El \gg 1$ ). Elasticity is defined as the ratio of the Weissenberg number to the Reynolds number. For shear banding wormlike micelle **solutions** where  $El \gg 1$ , a primary transition from the base Couette flow to stationary vortices that are evenly spaced in the axial direction of the shear cell and are characterized by an asymptotic wave-length is observed. The dimensionless wave-length at the onset of this shear banding transition for CTAB/NaSal system turns out to be much larger than those reported for other shear banding wormlike micelle systems. For the same fluid at a temperature where it shear-thins but does not display shear banding,  $El \approx 1$ , and for slow ramp speeds, the primary transition is to distinct structures that are not stationary but rather travel in the axial direction. At low elasticity ( $El \ll 1$ ), where the fluid behaves as a nearly Newtonian fluid, several transitions from purely azimuthal Couette flow to modified Taylor vortex flows and finally chaotic regimes are documented. The behavior in the shear-banding and non-shear-banding regimes are discussed and compared with results in related systems. The possibility of hysteresis in the flow transitions as well as the effects of co-rotation and counter-rotation of the cylinders on transitions and instabilities are also examined for a wide range of elasticity.

## I. INTRODUCTION

The hydrodynamic stability of Taylor-Couette flow, or flow between two concentric cylinders, has received considerable attention since the seminal work of G. I. Taylor [1]. The Taylor-Couette geometry is a versatile platform to study instabilities in flowing fluids and is characterized by the cylinder height  $h$ , inner cylinder radius  $R_i$ , and the outer cylinder radius  $R_o$ . In non-dimensional terms the geometry is parameterized in terms of an aspect ratio  $\Gamma = h/(R_o - R_i)$  and either a radius ratio  $R_i/R_o$  or a curvature ratio  $\varepsilon = (R_o - R_i)/R_i$ . G. I. Taylor presented a **groundbreaking** paper on the inertial instability of Newtonian fluids sheared in the concentric cylinders geometry and identified a critical threshold for the onset of the primary **inertial** instability; in the case of rotation of the inner cylinder only, this is now typically written as  $Ta_c = \varepsilon Re_i^2$ , where  $Re_i$  is a Reynolds number based on the inner cylinder.  $Re_i$  is defined as  $Re_i = \rho R_i \Omega_i (R_o - R_i)/\eta$ , where,  $\rho$ ,  $\Omega_i$ , and  $\eta$  are the density of the fluid, angular velocity of the inner cylinder, and viscosity of the Newtonian fluid, respectively. This instability is thus related to a coupling between inertial forces and streamline curvature [1]. Beyond this critical threshold the purely azimuthal base flow is replaced by an axisymmetric, time independent toroidal vortex flow, now referred to as Taylor Vortex Flow (TVF). Several other transitions follow as  $Re_i$  (or  $Ta$ ) is further increased, and eventually a Newtonian fluid **exhibits** a series of turbulent states. In a subsequent **important** study, Andereck and co-workers examined the effect of co-rotation and counter rotation of the cylinders on the Newtonian transitions and reported a wide variety of flow states and transitions [2]. Many excellent reviews on **Newtonian Taylor-Couette instabilities** exist and readers are encouraged to consult those [3–5].

There is also a rich literature on transitions and instabilities of viscoelastic polymeric fluids in the Taylor-Couette geometry [6–22]. Researchers have shown that addition of a small amount of polymer to Newtonian fluids dramatically alters the instabilities and transitions reported for Newtonian fluids in the Taylor-Couette **geometry** [15, 16]. Larson et al. [8] discovered a purely elastic instability in polymer solutions at vanishing Reynolds numbers. They proposed a criterion for the onset of elastic instability for an Oldroyd-B fluid based on a linear stability analysis as follows:

$$K_c \sim \varepsilon^{1/2} f(\eta_p/\eta_s) Wi, \quad (1)$$

where the Weissenberg number  $Wi$  is defined as the polymer relaxation time multiplied by the shear rate.  $\eta_p$  and  $\eta_s$  are the polymeric contribution to the viscosity and the solvent viscosity, respectively. This purely elastic instability is thus related to a coupling between elastic forces and streamline curvature. This work inspired many other studies that investigated different aspects of elastic instabilities of polymer solutions in the Taylor-Couette cell [10–12, 15, 17–19]. In addition, there have been many efforts to study the inertio-elastic instability in polymer solutions where both

Reynolds and Weissenberg numbers are important. One naturally expects the critical threshold for onset of inertio-elastic instability ( $S$ ) in polymeric fluids to depend on several parameters; at a minimum one would anticipate the following:

$$S \sim f(\varepsilon, \eta_p/\eta_s, Wi, Re). \quad (2)$$

The competition between elastic and inertial forces can be cast in a dimensionless elasticity number defined as  $El = Wi/Re$ . In the range of very low elasticity (i.e.  $El \ll 1$ ), researchers have primarily recovered transitions similar to Newtonian fluids, with the critical thresholds shifted slightly due to the presence of a small amount of elasticity [12, 13]. For example, Dutcher and Muller studied a dilute solution of polyethylene oxide (PEO) in glycerol/water and reported the same transition sequence as for Newtonian fluids, namely Couette flow (CF) to axisymmetric time independent vortex flow (TVF) to wavy vortex flow (WVF) for a range of  $10^{-4} < El < 0.02$ , and  $0.3 < \eta_p/\eta_s < 0.93$  [13]. **Similar results have been reported by Crumeyrolle and co-workers [12] and Groisman and Steinberg [17, 20], although the latter authors report a modified transition sequence under certain conditions of  $El$  and  $\eta_p/\eta_s$ .**

In the range of moderate elasticity ( $El \approx O(1)$ ), the transitions **observed for Newtonian fluids** are modified by elasticity and replaced by new transitions [12, 14]. **As an example,** for PEO/water solutions with PEO concentrations above 500 ppm, Crumeyrolle et al. reported a primary transition from Couette flow to **a new standing wave (SW) state** in the range of  $0.07 < El < 0.5$ , and  $5.32 < \eta_p/\eta_s < 12.4$  [12]. More recently, Dutcher and Muller reported **a different series of (non-Newtonian) transitions for a slightly shear-thinning PEO solution for  $El \approx 0.1$ -0.2 and found the transition sequence was hysteretic [21].** Groisman and Steinberg also studied instabilities in Taylor-Couette flow of a solution of polyacrylamide (PAAm) in a viscous sugar syrup (aqueous solutions of saccharose of different concentrations) systematically **and observed transitions at low  $El$  that were dependent on  $El$  and, for  $El > 0.3$  were hysteretic [15, 17–19].** Further detailed information on inertio-elastic instabilities in polymer solutions can be found in recent reviews [19, 22].

Most of the above experiments on viscoelastic polymer solutions have focused on inner cylinder rotation while the outer cylinder was held fixed. However, as in Newtonian fluids, the simultaneous rotation of both cylinders has a dramatic effect on transitions reported in polymeric fluids [13, 21]. Dutcher and Muller studied the effect of co- and counter rotation of cylinders over a modest range of elasticity for polymer solutions. For a dilute solution of PEO in water/glycerol and in the range of low elasticity  $El \approx 0.023$ , increasing co-rotation of the cylinders shifted the critical Reynolds number for the onset of instabilities to higher values. Moreover, Dutcher and Muller showed that for the range of moderate elasticity ( $El \approx 0.1$ -0.2), when cylinders rotate in counter fashion the **primary transition from CF is to disordered rotating standing waves (DRSW) rather than to stationary vortices** at high  $Re_o$  [13, 21].

Recently, surfactant based viscoelastic fluids (i.e. wormlike micellar fluids) have been widely used as model viscoelastic solutions for rheological studies [23]. These fluids are made by dissolving surfactants and salts in water. In contrast to polymer solutions that exhibit a spectrum of relaxation times, some wormlike micellar solutions follow a single mode Maxwell model in their linear viscoelastic behavior [24]. In the non-linear regime, they sometimes exhibit shear banding which is characterized by the formation of a plateau in the flow curve within a range of shear rates [23, 25–27]. In recent years, wormlike micelles have been used to study viscoelastic instabilities in different geometries such as Taylor-Couette cells, cross slots, microchannels and also in flow past an obstacle [26, 28–32]. In Taylor-Couette geometries, most of these studies are focused on the purely elastic instability and rotation of the inner cylinder only [28, 33–35]. Taylor-Couette studies by Fardin and co-workers have shown, for a broad range of shear-banding wormlike micelle systems in the high elasticity limit, a primary transition to Taylor-like vortices in the high shear band that causes the interface between the low and high shear bands to undulate. Near the critical conditions, these vortices oscillate in the axial direction and are characterized by a wave-length that scales with the thickness of the high shear band [26, 28, 33–35].

To the best of our knowledge, there is only one work that has reported an inertio-elastic instability for wormlike micelle solutions in the Taylor-Couette geometry, and there is as yet little data on flow transitions and instabilities over a wide range of elasticity in these solutions [36]. Perge et al. studied instabilities and transitions in a non-shear banding wormlike micelle system based on CTAB/NaNO<sub>3</sub> (0.1 M, 0.3 M) at moderate elasticity ( $El \approx 1$ ) and rotating only the inner cylinder [36]. Following a step-wise increment in  $Re_i$  they reported transitions similar to transitions reported for polymer solutions based on PEO/glycerol/water studied by Dutcher and Muller in the range of moderate elasticity  $El \approx 0.1$ -0.2 [21]. Perge et al. also showed that the primary transition is supercritical, and they observed no significant hysteresis for any of the transitions in their system. In contrast, Dutcher and Muller reported hysteresis in the critical conditions and flow states for viscoelastic solutions based on PEO/glycerol/water for  $El \approx 0.1$ -0.2 [21].

The main objectives of this work are as follows. First, we wish to examine systematically the inertio-elastic instability in a wormlike micellar fluid by varying the elasticity number over a wide range and examining any similarities or differences with results reported for polymer solutions. In contrast to polymeric solutions, wormlike micellar fluids are not susceptible to mechanical degradation and are much easier to prepare. Wormlike micelles can break and reform and this potentially leads to some differences with transitions reported for polymer solutions. This makes wormlike micelles perfect candidates to study hysteresis in Taylor-Couette flow. However, shear banding wormlike micelle solutions studied in the past were highly elastic and Taylor-Couette experiments always showed dominantly bulk, purely elastic instabilities. To vary the elasticity in wormlike micelle

**solutions** our approach is to change the temperature of the solution; in this regard, our approach is similar to that of Groisman and Steinberg [19] for polymer solutions. We note, however, that as we vary the temperature, we also vary the rheological behavior of the solutions, from shear-banding (at  $El \gg 1$ ) to shear-thinning with no shear-banding to nearly Newtonian behavior ( $El \ll 1$ ). Most of the wormlike micellar solutions studied in the past are thermo-thinning [37]. Increasing the temperature reduces the persistence length of the wormlike micelles and consequently the bulk viscosity and elasticity. However, it is quite challenging to find a wormlike micellar solution that allows us to **access** a wide range of rheological behaviors within the operating temperature range of our Taylor-Couette cell ( $20^\circ\text{C} < T < 40^\circ\text{C}$ ). It turns out that the wormlike micellar system based on CTAB/NaSal (0.075M,  $R = [\text{NaSal}]/[\text{CTAB}] = 0.32$ ) studied by Dubash et al. [29] allows us to study instabilities in a wide range of elasticity ( $O(10^{-3}) < El < O(100)$ ) within a narrow range of temperature ( $22^\circ\text{C} < T < 35^\circ\text{C}$ ). This enabled us to observe several interesting flow transitions in wormlike micelle **solutions** that have not been reported before, and to compare critical conditions to those in polymer solutions. Second, we note that we can introduce co- or counter-rotation of the cylinders. This broadens the range of flow transitions we can examine, and, in the case of counter rotation, allows us to change the characteristic length scale of the flow by introducing a nodal surface between the cylinders. This may potentially shift the thresholds of instabilities in flows of wormlike micelle **solutions**. To the best of our knowledge, the effects of co and counter rotation have not been studied for wormlike micellar systems over a wide range of elasticity.

## II. EXPERIMENTS

### A. Materials and Methods

The wormlike micelle **solution** studied in this work is an aqueous solution of cetyltrimethylammonium bromide (CTAB) and sodium salicylate (NaSal) (both supplied by Fischer Scientific). **Solutions** of 0.075 M CTAB and NaSal in de-ionized water with a ratio of  $[\text{NaSal}]/[\text{CTAB}] = 0.32$  **were prepared and mixed** with a magnetic stir bar. **Solutions** were left at room temperature for a few days to **allow** their equilibrium structure **to form prior to flow** experiments. For experiments in the Taylor-Couette cell a small amount of mica flakes (0.001 wt%, **Mearlin superfine, Mearl Corporation**) **were added** to **facilitate visualization** of the flow field. This small amount does not affect the rheology of the solution. Mica flakes are anisotropic particles that orient in the direction of flow, producing variations in the intensity of light reflected by ambient lighting and allowing us to monitor the formation and movement of vortex boundaries. Abcha and co-workers [38] have demonstrated that in the Taylor-Couette system the intensity of reflected light is directly related to the magnitude of the radial velocity component. **A Malvern Gemini stress-controlled rheometer was used** to characterize the rheology of the wormlike micelle **solution** at different temperatures, **in** both linear and non-linear viscoelastic shear experiments. The linear and non-linear tests are

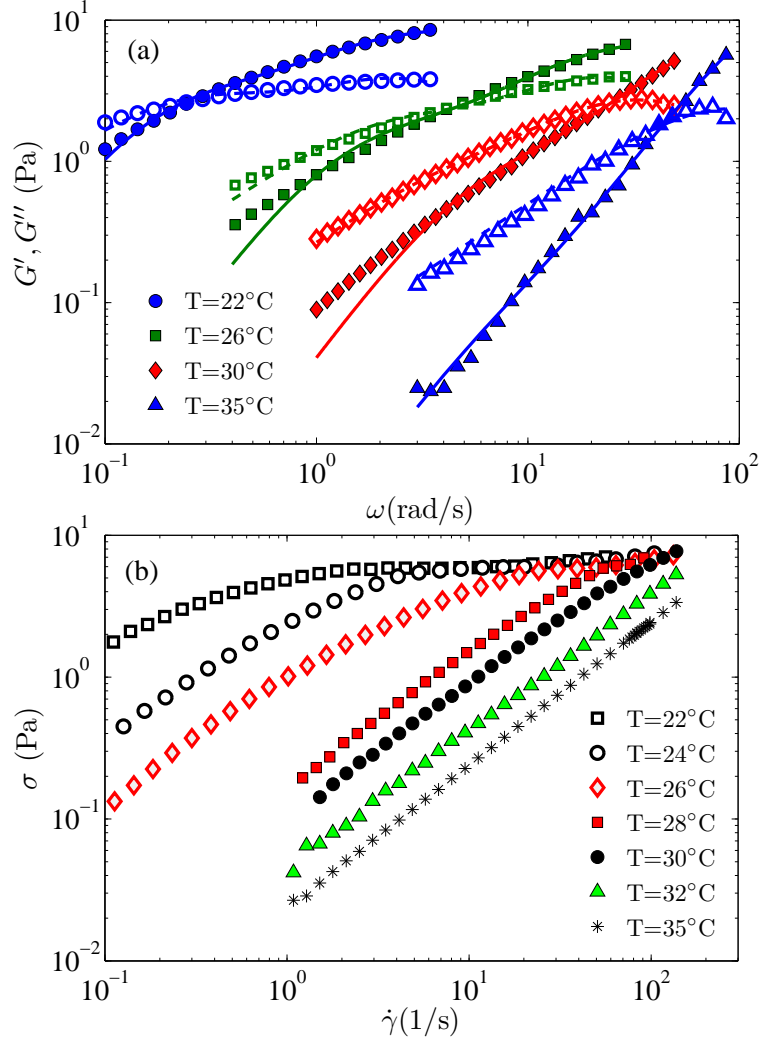


FIG. 1: **Rheology of surfactant micelle solutions:** (a) Storage (filled symbols) and loss moduli (open symbols) versus angular frequency. Curves show predictions of a two mode Maxwell model. (b) Shear stress versus shear rate for the range of temperature studied in this work **measured in a concentric cylinders geometry**. **Flow curves were obtained in strain controlled mode and for solutions the interval between each data point was set to 400 seconds to make sure the steady state is achieved.**

carried out in a Couette co-axial cylinders geometry with  $R_i = 1.25$  cm and  $R_o = 1.375$  cm. Flow measurements are carried out in a custom built, computer controlled Taylor-Couette cell that allows us to independently rotate both cylinders. The radii of the inner and the outer cylinders are 6.946 cm and 7.615 cm respectively, which provides a radius ratio of 0.91. The height of the Taylor-Couette cell is 40.6 cm corresponding to an aspect ratio of 60.7 that renders end effects negligible. The Taylor-Couette cell used in this study has been extensively used in the past for studies of flow transitions and instabilities [10, 11, 14]. Images of the variations in the light intensity in the  $\theta - z$  plane of the Taylor-Couette cell are captured using a CCD camera (model COHU 4910, **COHU, Inc.**) under ambient light exposure. Details of the Taylor-Couette cell, image capture, and image

processing may be found in [39].

### III. RESULTS AND DISCUSSION

#### A. Fluid Characterization

The system of wormlike micelles based on CTAB/NaSal used in this work has been studied by other researchers in microfluidic studies [29]. This solution is very sensitive to small variations in temperature. Small amplitude oscillatory shear experiments were performed to extract the longest relaxation time  $\tau_M$  of the fluid. Fig. 1(a) shows typical linear viscoelastic results along with the prediction of a two mode Maxwell model (eq. (3) and (4)) at different temperatures. We note that a single mode Maxwell model does not fit well **the measured fluid response**. This is consistent with the findings of Dubash et al. for the linear viscoelastic results of solutions based on CTAB/NaSal in the concentration range studied in this work [29].

$$G'(\omega) = \sum_{i=1}^2 \frac{\tau_i^2 \omega^2}{1 + \tau_i^2 \omega^2} G_{oi} \quad (3)$$

$$G''(\omega) = \sum_{i=1}^2 \frac{\tau_i \omega}{1 + \tau_i^2 \omega^2} G_{oi} \quad (4)$$

Similarly, it has been shown that **other** surfactant-based viscoelastic solutions depart from ideal, single mode Maxwell behavior as the concentration decreases from well inside the semi-dilute regime towards the dilute regime [40]. Steady shear experiments were also performed to measure the shear stress  $\sigma$  as a function of the shear rate at different temperatures (cf. Fig. 1(b)). At the lowest temperature tested in this work ( $T = 22^\circ\text{C}$ ), the shear banding plateau is evident, however increasing the temperature causes the wormlike micelle **solution** to become **a** non-shear banding viscoelastic fluid over an intermediate range of temperature ( $26^\circ\text{C} - 32^\circ\text{C}$ ) and eventually to behave as a nearly Newtonian fluid (non-shear-thinning, and only very weakly elastic) at the maximum temperature ( $T = 35^\circ\text{C}$ ). **At  $T = 22^\circ\text{C}$ , the lower and the upper limits of the shear banding plateau are  $\dot{\gamma}_l = 3.25 \text{ s}^{-1}$  and  $\dot{\gamma}_h = 14.2 \text{ s}^{-1}$ , respectively. At  $T = 24^\circ\text{C}$ , these values are  $\dot{\gamma}_l = 9 \text{ s}^{-1}$  and  $\dot{\gamma}_h = 30.75 \text{ s}^{-1}$ . This is best shown when the data in Fig. 1 (b) are replotted on semi-log coordinates (cf. Fig. S1 in [41]).**

The fluid properties, including the longest Maxwell relaxation time  $\tau_M$ , the zero shear rate viscosity  $\eta_0$ , the power law index  $n$ , viscosity ratio  $\eta_p/\eta_s$  and the Elasticity number  $El = Wi/Re_i$ , as a function of temperature  $T$  are summarized in Table I.  **$\eta_s$  represents the solvent (water) viscosity ( $10^{-3} \text{ Pa.s}$ ).  $\eta_p(\dot{\gamma})$  is defined as the contribution of the wormlike micelles to the surfactant solution viscosity ( $\eta_p(\dot{\gamma}) = \eta(\dot{\gamma}) - \eta_s$ ).  $\eta(\dot{\gamma})$  is the total wormlike micelles solution viscosity measured in**



T (°C)	$\tau_M$ (s)	$\eta_0$ (Pa.s)	$\eta_p/\eta_s$	$El$
22	4.52	17.4	850 – 1340	15.5 – 18.6
24	2.55	2.3	400 – 600	3.3 – 4.2
26	0.88	1.2	270 – 380	0.72 – 0.97
28	0.54	0.16	130	0.2
30	0.165	0.08	70	0.034
32	0.11	0.04	39	0.01
35	0.04	0.025	23	0.003

TABLE I: List of surfactant solution properties for the range of temperatures tested in this work.

the rheometer. Here we define the Weissenberg number  $Wi$  as  $Wi = \tau_M \dot{\gamma}_i$  where  $\dot{\gamma}_i$  is the imposed shear rate, calculated as  $\dot{\gamma}_i = |R_o \Omega_o - R_i \Omega_i|/d$ . The Reynolds number based on the inner cylinder is defined as  $Re_i = \rho \Omega_i R_i d / \eta(\dot{\gamma}_i)$ , where  $d$  is the gap between the cylinders,  $d = R_o - R_i$ . The full results of our two-mode Maxwell model fit are included in Table SI of supplementary material. We note that for all temperatures below 28°C, the viscosity is shear rate dependent, and hence  $El$  varies with imposed shear rate; the range of  $El$  accessed in the present work is indicated in Table I.

As noted above, the characteristic shear rate is defined as the imposed shear rate, consistent with earlier studies and with the rheological data. However, most of the solutions studied in the present work are shear thinning or shear banding and this definition does not account for the effect of shear thinning on the base velocity field. Although the imposed shear rate provides a good approximation for the flow of the shear banding fluid at the beginning of the shear banding plateau (cf. Fig. S3 in [41]), for higher shear rates that are within the shear banding regime, the imposed shear rate underestimates the local shear rate in the high shear band. On the other hand, the shear rate profile based on the shear thinning power-law fluid often overestimates the shear rate in the high shear band (cf. Fig. S4 in [41]). Thus, while the imposed shear rate is not necessarily equal to the local shear rate at the inner cylinder, we use it to be consistent with the literature results and the rheological measurements.

## B. Flow Transitions and Instabilities

In this section, we present results that illustrate the flow transitions and instabilities for our wormlike micellar fluid in the Taylor-Couette cell as the temperature, and hence  $El$  and rheological properties, are varied. The inner cylinder rotation is slowly ramped at a rate of 0.001 rad/s<sup>2</sup> in all experiments, so that flows at increasing  $Re_i$  and  $Wi$  are accessed for  $Re_o = 0$  (that is, the outer cylinder is held stationary). We performed many experiments to establish that this ramp rate is sufficiently slow that neither the critical conditions nor the flow state observed were changed



by using a slower ramp rate. Note that since the viscosity is shear rate dependent (at all except for the highest temperatures), the Elasticity number varies modestly during the ramp. Images of the  $\theta - z$  plane of the TC geometry are captured using a CCD camera. A single line of pixels is selected in the axial direction of the TC cell for each shear rate and collected over time (as  $Re_i$  is slowly increased) to form space-time (or space- $Re_i$ ) plots. The space-time plot is a useful way to determine the  $Re_i$  corresponding to the onset of flow transitions and instabilities, and has been used extensively in the literature [12, 14, 15]. In the following, we present such results for the same wormlike micellar solution as it displays shear banding (and high  $El$ ), shear-thinning viscoelastic behavior (at moderate  $El$ ), and nearly Newtonian behavior (at  $El \ll 1$ ) in steady shear rheology.

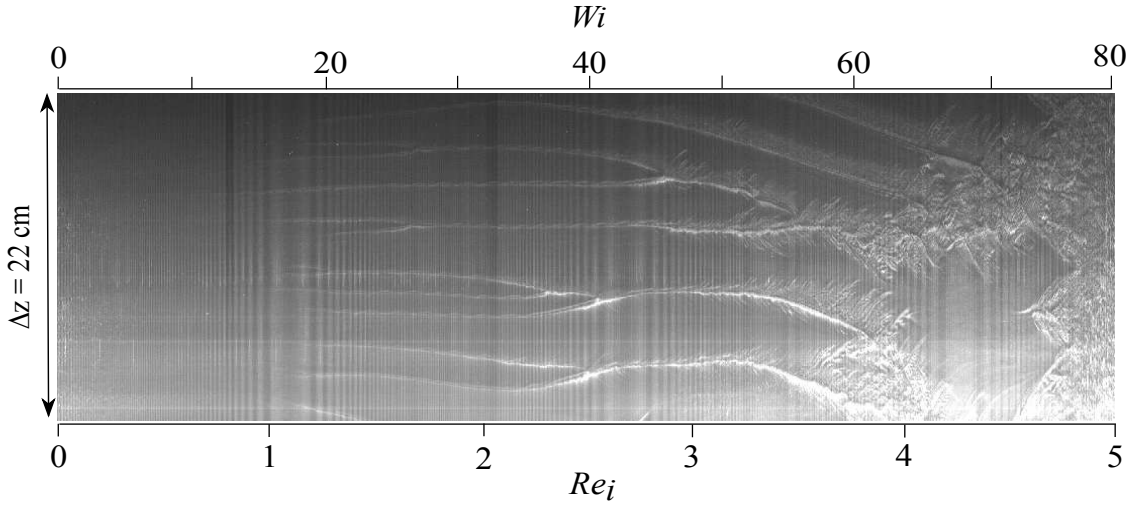


FIG. 2: Space-time diagram of CTAB/NaSal at  $T = 22^\circ\text{C}$  during a gradual acceleration ( $0.001 \text{ rad/s}^2$ ) from rest to a shear rate of  $17.7 \text{ s}^{-1}$ . The vertical stripes in the image are caused by the temporal variation of the light source.

### 1. Shear banding regime

At low temperatures (e.g.  $T = 22^\circ\text{C}$ ,  $T = 24^\circ\text{C}$ ), rheological measurements indicate that the wormlike micellar solution exhibits shear banding. Fig. (2) shows the space-time plot of this shear banding wormlike micellar fluid at  $T = 22^\circ\text{C}$  with increasing  $Re_i$ . We report the initial formation of stationary vortices at  $Re_i = 0.85$ ,  $Wi = 15.8$ , and  $El = 18.6$  signaled by the presence of horizontal lines on the space-time plot, and characterized by an initial dimensionless axial wavelength of  $\approx 2.3$ . The dimensionless wavelength,  $\lambda$ , is defined as the wavelength over the gap size  $d$  and the wavelength is calculated as the spacing between the bright bands shown in Fig. (2). These bands merge and form stationary structures characterized by a larger axial wavelength as we increase the  $Re_i$ . Finally, we report a transition from evenly spaced bright bands denoting stationary vortices to a chaotic regime which is reminiscent of elastic turbulence at  $Re_i = 2.9$ ,  $Wi = 44.9$  and  $El =$

15.5. The vertical stripes evident in Fig. (2) and subsequent space-time plots are due to small temporal fluctuations in the intensity of the light source.

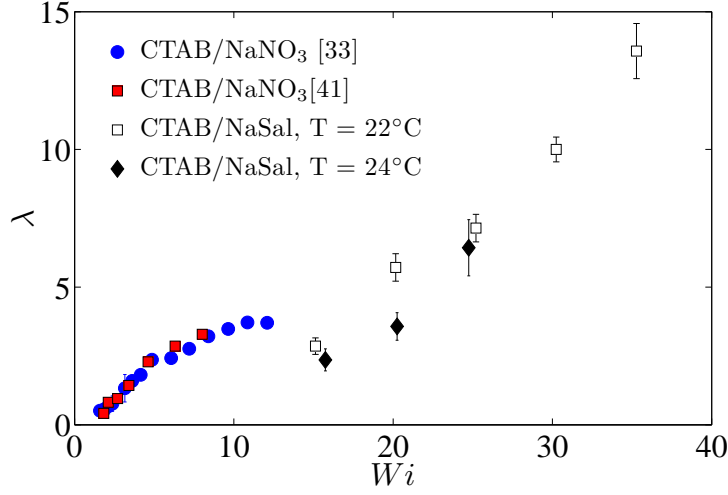


FIG. 3: Dimensionless wavelength versus Weissenberg number for different wormlike micelle solutions.

Fig. (3) shows the dimensionless wavelength ( $\lambda$ ) versus Weissenberg number ( $Wi$ ) for our experiments on the CTAB/NaSal system along with the results for the CTAB/NaNO<sub>3</sub> wormlike micellar fluid studied by Lerouge and co-workers. We also include data from our own laboratory for the CTAB/NaNO<sub>3</sub> system [44], which coincides with the published results of Lerouge and co-workers [28]. As shown in Fig. (3), the results for CTAB/NaSal show some differences with the CTAB/NaNO<sub>3</sub> system in terms of the critical  $Wi$  for the onset of instability (inferred from Fig. (3)) and the wavelengths for the range of  $Wi$  tested.

The elasticity number for the transition from Couette flow to stationary vortices as well as from stationary vortices to elastic turbulence is high ( $\gg 1$ ) for the CTAB/NaSal system, and it appears to follow the purely elastic pathway. The first transition occurs at an imposed shear rate just above the start of the shear banding plateau. The purely elastic criterion indicated in eq. (1) is modified by Fardin et al. for shear-banding systems (cf. eq. (1) in [42]) to account for the Weissenberg number  $Wi_h$  in the high shear band and the proportion of that band in the gap  $\alpha$  as  $K_c \sim (\alpha\varepsilon)^{1/2}Wi_h$ . Here,  $Wi_h$  is given by the longest relaxation time multiplied by the shear rate in the high shear rate band. The proportion of the high shear band is estimated using the lever rule:

$$\dot{\gamma} = \alpha\dot{\gamma}_h + (1 - \alpha)\dot{\gamma}_l, \quad (5)$$

where  $\dot{\gamma}_l$  and  $\dot{\gamma}_h$  are the shear rates for onset of the shear banding plateau and the end of the shear banding respectively. We note that this equation neglects the effects of shear-thinning.

Our critical condition for the first transition of  $Wi \approx 15.8$  at  $T = 22^\circ\text{C}$  corresponds to a

critical condition  $K_c \sim (\alpha\varepsilon)^{1/2}Wi_h \approx 3$ . Fardin et al. [43] showed that for the shear banding system of CTAB/NaNO<sub>3</sub>, the critical condition for onset of elastic instability is  $K_c \approx O(1)$ . This is also consistent with our measurements for the CTAB/NaNO<sub>3</sub> system, as suggested by Fig. 3.

Thus, the critical condition for onset of the elastic instability in CTAB/NaSal differs **modestly** from that for the CTAB/NaNO<sub>3</sub> system, and we note that at onset, the CTAB/NaSal system displays a higher dimensionless wavelength than the CTAB/NaNO<sub>3</sub> system. We note a few potential sources for these discrepancies in  $K_c$  and the wavelength at onset. First, wall slip at the moving boundary might in principle affect the values of  $K_c$ . It has been shown that the shear banding system based on CTAB/NaNO<sub>3</sub> experiences significant wall slip at the onset of shear banding [33]. Fardin et al. [43] showed that the local  $Wi_h$  measured via velocimetry techniques is typically lower than the global  $Wi_h$  measured with a commercial rheometer for the beginning of the shear banding regime. In particular, the local  $Wi_h$  at the onset of shear banding in their case is almost 1/3 of the globally measured  $Wi_h$ , and they used this locally measured  $Wi_h$  to calculate the critical threshold for onset of elastic instability. Although there are no direct measurements of slip for the CTAB/NaSal system, slip might potentially lower the effective shear rate at the inner cylinder of our Taylor-Couette geometry and this in turn would change the local  $Wi_h$ , the value of  $\alpha$  and thus  $K_c$ . Second, although the shear banding wormlike micellar solution studied in this work at  $T = 22^\circ\text{C}$  shows no significant qualitative differences in terms of non-linear rheology with the CTAB/NaNO<sub>3</sub> shear banding wormlike system studied before [33, 34], quantitative differences exist. For example, the linear viscoelasticity results for CTAB/NaSal are best fit with a two mode Maxwell model, whereas, for CTAB/NaNO<sub>3</sub>, a single mode Maxwell model gives the best fit. The differences between the two shear banding systems in linear viscoelasticity tests presumably arise from different wormlike micellar structures. Therefore, in addition to wall slip, this factor might also lead to differences in the critical values  $K_c$  and  $\alpha$  at the onset of the purely elastic instability for the two systems mentioned above. **We also note that, for polymer solutions, the value of the critical condition and the axial wavelength of the purely elastic instability are sensitive to viscosity ratio and to shear thinning, with the dimensionless wavelength increasing with increased shear thinning [7]; thus, differences between these quantities for the two wormlike micelle systems may also be playing a role.**

## 2. Viscoelastic regime

At higher temperatures, the CTAB/NaSal surfactant solution no longer shows any sign of shear banding. Instead, the rheological measurements show that it remains viscoelastic for the range of temperature  $26^\circ\text{C} < T < 32^\circ\text{C}$ . In this intermediate elasticity regime, flow visualization in the Taylor-Couette cell reveals new transitions that differ from those of shear banding fluids and from those reported for weakly elastic polymer solutions [12, 13]. Fig. (4) illustrates regimes

of the surfactant solution at different temperatures within the range 26 - 32°C, where the fluid shear-thins but displays no shear-banding. As the temperature is varied over this interval range, the elasticity number changes from approximately 1 to 0.01.

At  $T = 26^\circ\text{C}$ , where  $El \approx 1$ , travelling waves that typically originate at the middle of the cylinders and move towards both the top and bottom of the cylinders form (c.f. Fig. 4(a)) at  $Re_i \approx 11.4$  and  $Wi \approx 11.3$ . The primary transition from Couette flow is thus no longer to stationary secondary flows; we refer to these structures as travelling vortices (TV). The corresponding elasticity number for the onset of transition from Couette flow to travelling vortices is about  $El \approx 0.97$ . To the best of our knowledge, this flow transition to travelling vortices is reported for a surfactant based viscoelastic fluid for the first time. With increasing  $Re_i$ , these travelling vortices are replaced near  $Re_i \approx 27.2$ ,  $Wi \approx 18.5$  by a chaotic regime that is reminiscent of elastic turbulence. Perge et al. [36] also studied the transitions in flow of a non-shear banding viscoelastic micellar system based on CTAB/NaNO<sub>3</sub> in the same range of elasticity ( $El \approx 1$ ) and reported transitions as: CF  $\rightarrow$  standing waves (SW)  $\rightarrow$  rotating standing waves (RSW)  $\rightarrow$  elastic turbulence (ET) with increasing  $Re_i$ . These authors reported the critical condition for the primary transition as  $Re_i \approx 68$ ,  $Wi \approx 75$  for their geometry in which  $\varepsilon = 0.087$ . We can account for the slight difference in curvature between their geometry and ours (for which  $\varepsilon = 0.0963$ ) by casting the critical conditions in terms of inertial and elastic Taylor numbers where  $Ta_i = \varepsilon Re^2$  and  $Ta_e = \varepsilon Wi^2$  respectively. However, even accounting for the small difference in curvature, the critical conditions for the first transition (and the form of the secondary flow) differ dramatically for the two systems. We note that the viscosity ratio for the onset of transition from CF  $\rightarrow$  SW, in the system studied by Perge et al. [36] is approximately 50, whereas, in this study the viscosity ratio for the onset of the first transition is approximately 380. The results of Perge and co-workers are similar to transitions reported for polymeric solutions based on PEO/glycerol/water by Dutcher and Muller in the range of elasticity of  $El \approx 0.1 - 0.2$  and viscosity ratio of 2.82 [21]. However, a different transition sequence is observed for the present CTAB/NaSal system at elasticity in this range. This might be due to the difference between the viscosity ratios, ramp protocol and/or the structure of wormlike micelles studied in this paper and those studied by Perge et al. [36]. Perge et al. [36] performed their experiments by step increases in shear rate, whereas in this study the ramp protocol is continuous and very slow (0.001 rad/s<sup>2</sup>). One would expect that a step or rapid ramp could easily result in anomalously high critical conditions (if the flow has insufficient time to develop) or forcing of the system into alternate, nonlinear flow states.

As the temperature is increased to  $T = 28^\circ\text{C}$ , the first transition from Couette flow to disordered oscillations (DO) is observed at  $Re_i \approx 66.7$ , for elasticity of about  $El \approx 0.2$  and the viscosity ratio of 130 (c.f. Fig. 4(b) and Table I). For solutions of linear, flexible polymers, the transition sequence in this range of  $El$  appears sensitive to the viscosity ratio  $\eta_p/\eta_s$ . Groisman and Steinberg reported

transition from Couette flow to disordered oscillations for a shear thinning viscoelastic solution based on PAAm/saccharose/water at  $El \approx 0.2 - 27$  and viscosity ratio of 0.82 [19]. However, Crumeyrolle et al. reported a transition from Couette flow to rotating standing waves in the moderate range of elasticity (0.07-0.5) for a series of PEO/water solutions with viscosity ratios in the range of 5 - 13 [12]. Additionally, Dutcher and Muller, for  $El \approx 0.1 - 0.2$ , reported transitions from Couette flow to stationary vortices to disordered rotating standing waves to elastic turbulence for a PEO/glycerol/water solution with a viscosity ratio of 2.8 [21].

Fig. 4(c) shows the rotating standing waves (RSW) transition and the disordered oscillations (DO) at  $T = 30^\circ\text{C}$ . These transitions correspond to elasticity of about  $El \approx 0.034$  and the viscosity ratio 69. Groisman and Steinberg showed for the system of PAAm/saccharose/water in the range of  $0.023 < El < 0.33$  and viscosity ratio of 0.78, that Couette flow is followed by rotating standing waves and then disordered oscillations. Our results indicate similar transitions for viscoelastic surfactant solutions in this range of elasticity. However, our results seem to be at odds with other experiments on linear, flexible polymer solutions of PEO in the low elasticity range, which report a primary transition to TVF, followed by wavy vortex flow [12, 13].

Finally, at  $T = 32^\circ\text{C}$ , the surfactant solution is slightly shear thinning ( $n = 0.95$ ) and the following transition sequences are observed: Couette flow to Taylor vortex flow to rotating standing waves to disordered oscillations. This experiment corresponds to elasticity of about  $El \approx 0.01$  and the viscosity ratio of 39. For solutions of linear, flexible polymers, the viscosity ratio again appears to play a role in the transition sequence. A sequence similar to the one we observe for our surfactant system was reported by Groisman and Steinberg for  $0.03 < El < 0.08$  and viscosity ratio of  $\eta_p/\eta_s \sim 0.82$  for PAAm/saccharose-water solutions [16]. However, Crumeyrolle et al. recovered the Newtonian, inertial sequence of transitions for the range of  $0.002 < El < 0.03$  and viscosity ratios of  $\eta_p/\eta_s = 0 - 3.45$  for PEO/water solutions [12]. In addition, Dutcher and Muller reported primarily Newtonian transitions for  $El \leq 0.023$  (Couette Flow to TVF to WVF) with thresholds being slightly shifted due to presence of elasticity [13]. Thus, while at  $El \sim 0.2$  ( $T = 28^\circ\text{C}$ ) the CTAB/NaSal solution displays a transition sequence similar to that observed in PEO [21], at  $0.001 < El < 0.2$  ( $28^\circ\text{C} < T < 32^\circ\text{C}$ ), the transition sequence follows that observed in PAAm solutions [16, 19]. In both PEO and PAAm the sequence is sensitive to viscosity ratio, and the CTAB/NaSal viscosity ratio is much larger than in earlier experiments with PEO and PAAm.

### 3. Newtonian regime

The surfactant solution exhibits nearly Newtonian behavior in steady shear rheology at  $T = 35^\circ\text{C}$  (almost no discernible shear-thinning and a very low relaxation time) and the inertial sequence of



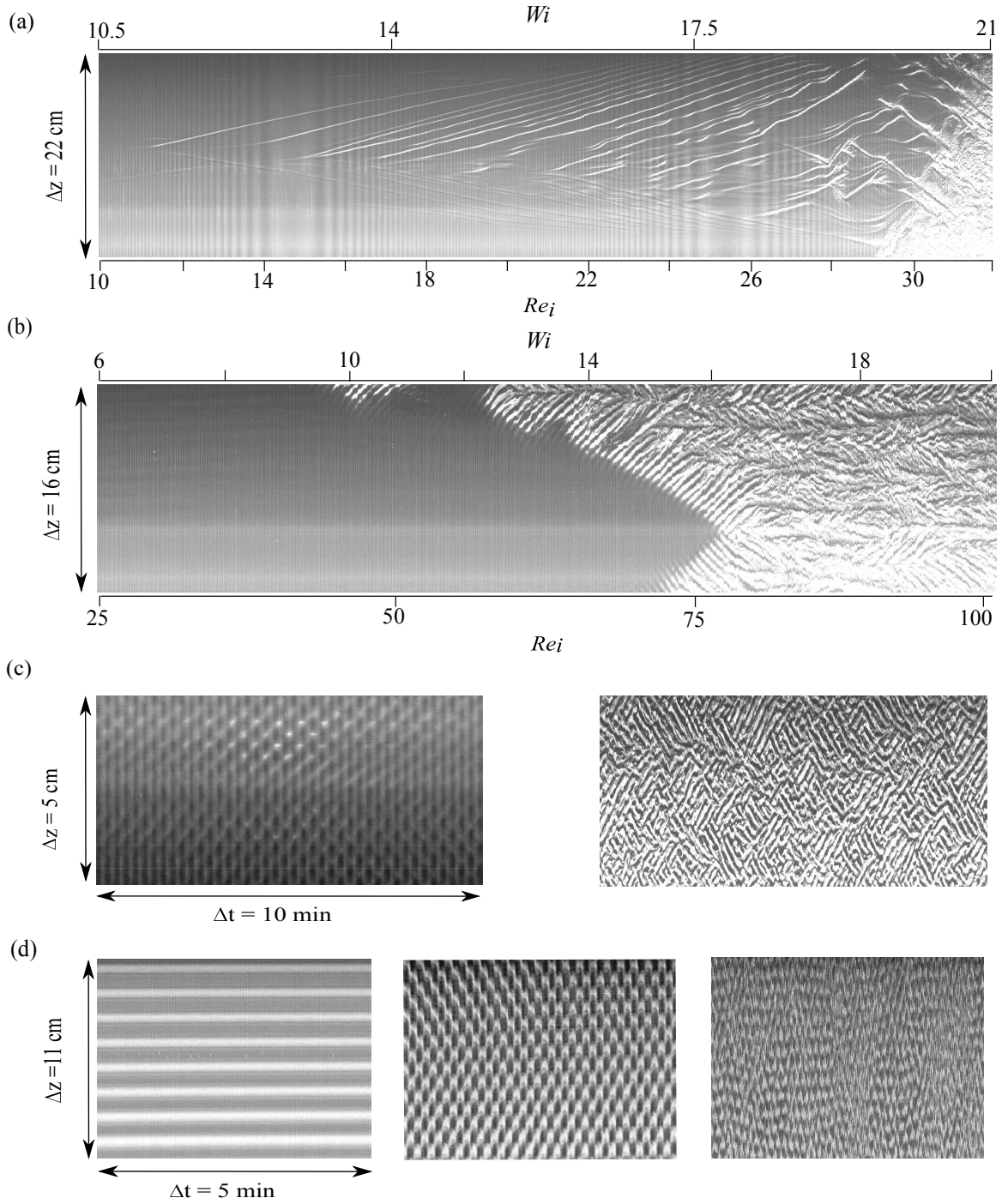


FIG. 4: Space-time plots of CTAB/NaSal system at different temperature showing: (a) Couette flow to traveling vortices ( $Re_i \approx 11.4$ ) to elastic turbulence transition ( $Re_i \approx 27.2$ ) at  $T = 26^\circ\text{C}$  and  $El \approx 0.97 \rightarrow 0.72$ . (b) Couette flow to disordered oscillations ( $Re_i \approx 66.7$ ) at  $T = 28^\circ\text{C}$  and  $El \approx 0.2$ . (c) rotating standing waves ( $Re_i \approx 79.7$ ) to disordered oscillations ( $Re_i \approx 96.5$ ) at  $T = 30^\circ\text{C}$  and  $El \approx 0.034$ . (d) Taylor vortex flow ( $Re_i \approx 142.7$ ) to rotating standing waves ( $Re_i \approx 151.3$ ) to disordered oscillations ( $Re_i \approx 179.5$ ) at  $T = 32^\circ\text{C}$  and  $El \approx 0.01$ . Experiments were conducted using a gradual acceleration ( $0.001 \text{ rad/s}^2$ ) from rest.

transitions **observed for Newtonian fluids** are also recovered in the flow visualization experiments in the Taylor-Couette cell. These **experiments** correspond to elasticity of about  $El \approx 0.003$ . Fig. 5 shows space-time plots for the first three flow states following Couette flow observed for the surfactant solution at  $T = 35^\circ\text{C}$ . This is consistent with the results reported on both polymer solutions and Newtonian fluids [12, 13].

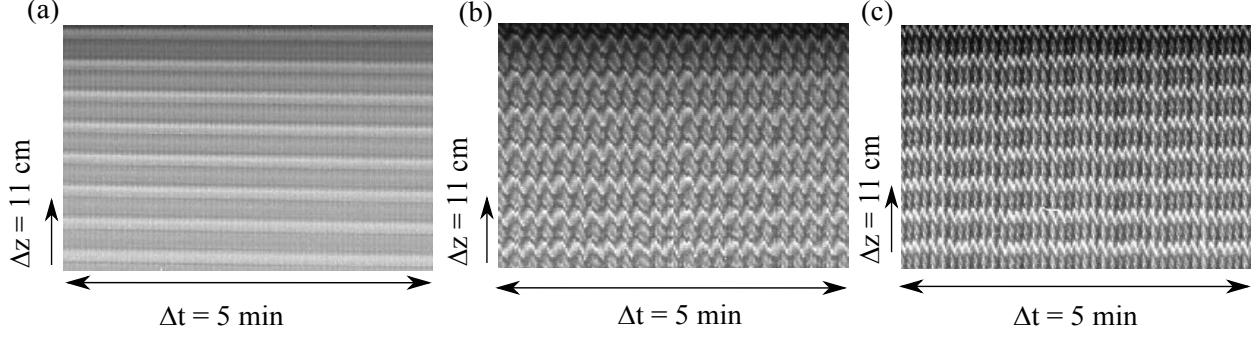


FIG. 5: (a) Taylor Vortex Flow ( $Re_i \approx 136$ ), (b) Wavy Vortex Flow ( $Re_i \approx 157.3$ ) and (c) Modulated Wavy Vortex Flow ( $Re_i \approx 181.5$ ) for the surfactant solution at  $T = 35^\circ\text{C}$  and  $El \approx 0.003$ . **Experiments were conducted using a gradual acceleration ( $0.001 \text{ rad/s}^2$ ) from rest.**

Finally, Fig. (6) summarizes all of the above results in terms of three dimensionless parameters:  $Re_i/Re_N$ ,  $Wi$  and  $El$ .  $Re_N$  denotes the onset of the TVF transition for a Newtonian fluid in our Taylor-Couette cell ( $Re_N \approx 140$ ). In Fig. (6) we have also specified three regimes (I-III) for which the surfactant solution shows different rheological responses. In general, the rise in temperature from  $T = 22^\circ\text{C}$  to  $T = 35^\circ\text{C}$  lowers the elasticity (c.f. Fig. 6(a)) which in turn shifts the onset of instabilities to higher  $Re_i/Re_N$ . As we approach the Newtonian behavior ( $T \rightarrow 35^\circ\text{C}$ ), the onset of the first transition gradually increases till it reaches values near unity ( $Re_i/Re_N \approx 0.97$ ). We also note that at the lowest temperature - where the fluid is strongly shear thinning- the critical elasticity numbers for the primary and secondary transitions are varying as we ramp in  $Re_i$  and as we increase the temperature, this difference is weakened until it becomes negligible at  $T = 32^\circ\text{C}$  **where the shear-thinning is very modest**. However, increasing the temperature has the opposite effect on the critical Weissenberg number for the onset of instabilities. As the temperature decreases ( $T \rightarrow 22^\circ\text{C}$ ), the critical  $Wi$  for onset of first transition increases and finally, in the range of high elasticity (i.e. lowest temperature) when the elastic instability is dominant, it reaches a constant value of  $Wi \approx 15 - 17$ . This monotonic trend is consistent with prior experimental results on PAAm/saccharose/water solutions by Groisman and Steinberg for which an asymptotic value of  $Wi \approx 25$  was recovered [19].



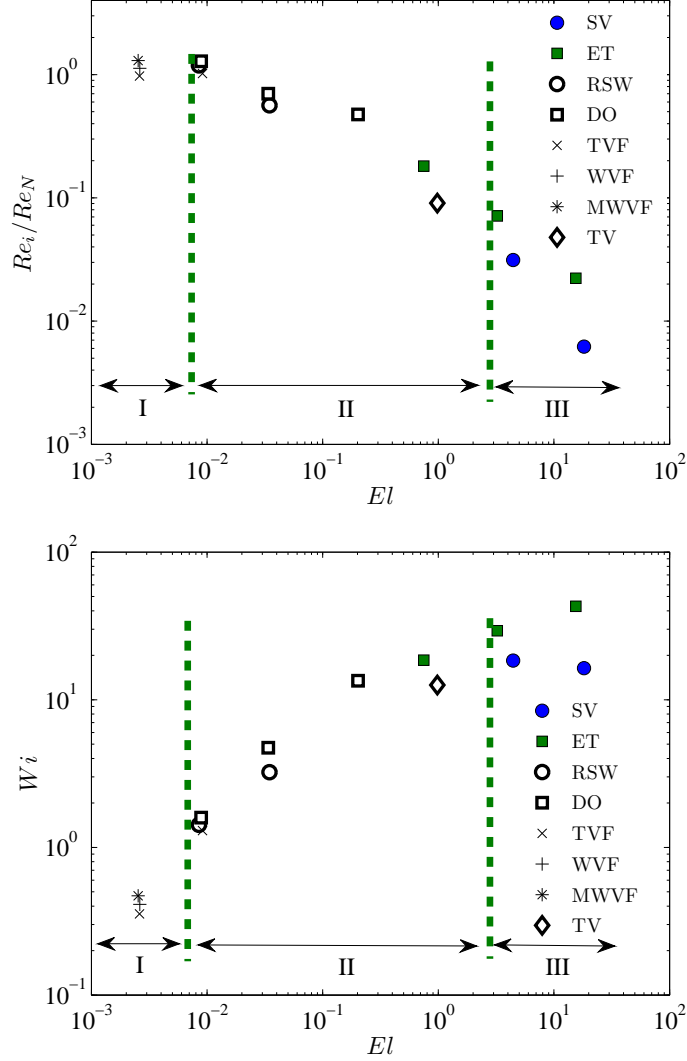


FIG. 6: (a) Dimensionless Reynolds versus Elasticity number for different flow transitions with increasing  $Re_i$ . (b) Weissenberg number versus Elasticity for all flow transitions. The following transitions: • (stationary vortices), ■ (elastic turbulence), ○ (rotating standing waves), □ (disordered oscillation), × (Taylor vortex flow), + (wavy vortex flow), \* (modulated wavy vortex flow) and ◇ (traveling vortices) are reported in the range of temperature 22-35 °C. Regimes I-III correspond to Newtonian, shear thinning viscoelastic and shear banding rheology respectively.

### C. Effect of the Flow History

Flow transitions and the final flow state at a particular set of parameters for viscoelastic polymer solutions might in principle be affected by the flow history. Such flow state hysteresis is well-known for wavy vortex flow of Newtonian fluids as first revealed by Coles [44]. Although hysteresis has been reported in the Taylor-Couette flow of polymeric solutions [19, 21], wormlike micellar solutions based on CTAB/NaNO<sub>3</sub> showed no sign of hysteresis in the studies of Perge et al. [36]

for the moderate range of elasticity ( $El \approx 1$ ). We also report no sign of hysteresis for flow of wormlike micelles based on CTAB/NaSal in the range of high and moderate elasticity  $El \geq 1$  for the transitions indicated in Fig. (6). However, for elasticity of  $El \approx 0.2$  and  $El \approx 0.034$  we report a transition similar to solitary vortex pairs (diwhirls) as we decrease the  $Re_i$ . Fig. (7) shows the transition from DO to oscillatory strips to solitary vortex pairs (diwhirls) to Couette flow at  $T = 28^\circ\text{C}$  ( $El \sim 0.2$ ) as  $Re_i$  decreases (compare this to the pathways shown in Fig. (6) where  $Re_i$  is increasing). If the spacing between the bright bands (which appear in Fig. (7) approximately over the range  $50 < Re_i < 28$ ) is small ( $< 5d$ ), they merge and form one bright strip similar to the behavior of solitary vortex pairs reported by Groisman and Steinberg [18]. If the pairs are far apart from each other ( $> 10d$ ), they do not interact with each other. Here,  $d$  represents the gap of our Taylor-Couette cell ( $d = 0.7\text{cm}$ ). For higher temperatures  $T \geq 32^\circ\text{C}$  that correspond to elasticity of  $El < 0.01$ , no signs of hysteresis were observed.

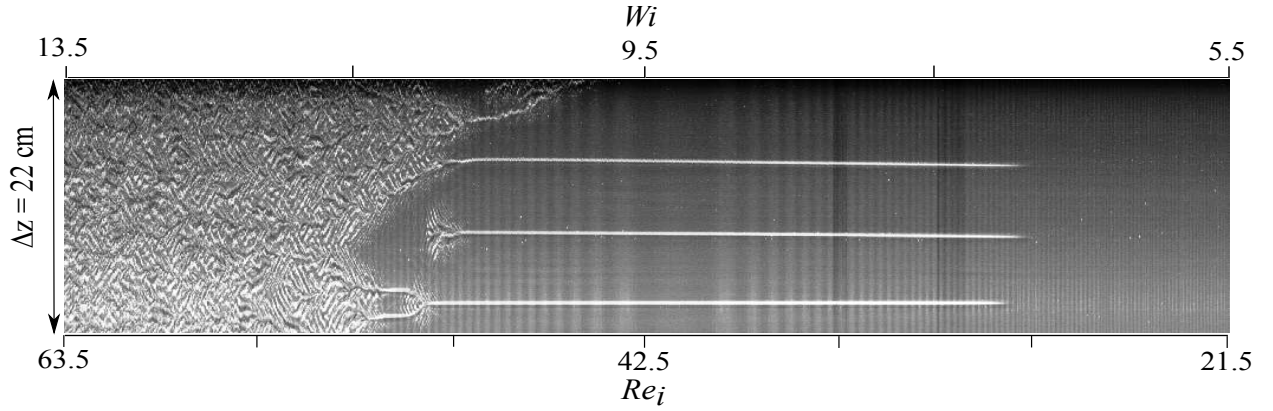


FIG. 7: Space-time plot for the surfactant solution at  $T = 28^\circ\text{C}$ ,  $El \approx 0.2$  with  $Re_i$  (lower bar) and  $Wi$  (upper bar) decreasing from left to the right. Experiments were conducted using a gradual deceleration ( $0.001 \text{ rad/s}^2$ ).

#### D. Effects of Co-rotation and Counter-rotation

Rotation of the outer cylinder can have a dramatic effect on flow instabilities and transitions. Counter rotation of the cylinders creates a nodal surface within the gap of the Taylor-Couette geometry at some radial position  $r = R_n$  (where  $R_i < R_n < R_o$ ) where the velocity is zero. This surface divides the gap into an inner and an outer part. The inner part can be thought of as a Taylor-Couette geometry defined by the rotating inner cylinder and a stationary outer boundary defined by the nodal surface. However, for the outer part, the inner boundary is defined by the stationary nodal surface while the outer cylinder is moving. Dutcher and Muller extensively studied co- and counter rotation of the cylinders on flow transitions for a PEO/glycerol/water solution at low elasticity  $El = 0.023$ . They reported that both co- and counter rotation shifts the

critical Reynolds numbers  $Re_i$  for the onset of both the primary and secondary instabilities (to TVF and WVF, respectively) to higher values, consistent with trends for Newtonian fluids [13]. They also observed similar trends for the onset of the first two instabilities in the range of moderate elasticity ( $El \approx 0.1 - 0.2$ ), although in this case the minimum in  $Re_i$  is shifted from  $Re_o = 0$  to  $Re_o \approx 30$  and the first transition is to elastically modified stationary vortices, and the second transition is to disordered rotating standing waves [21]. For wormlike micelles however, there are no experimental studies that examine the effect of rotation of the outer cylinder. In the following experiments, the outer cylinder is rotated quickly to reach its final value and then rotation of the inner cylinder is gradually ramped at a rate of  $0.001 \text{ rad/s}^2$ , increasing the inner cylinder angular velocity until we reach the instability thresholds. For co- and counter-rotation, we define  $Re_i = \rho R_i \Omega_i (R_o - R_i) / \eta (\dot{\gamma}_i)$  and  $Re_o = \rho R_o \Omega_o (R_o - R_i) / \eta (\dot{\gamma}_o)$  to be the Reynolds number at the inner and outer cylinders respectively.

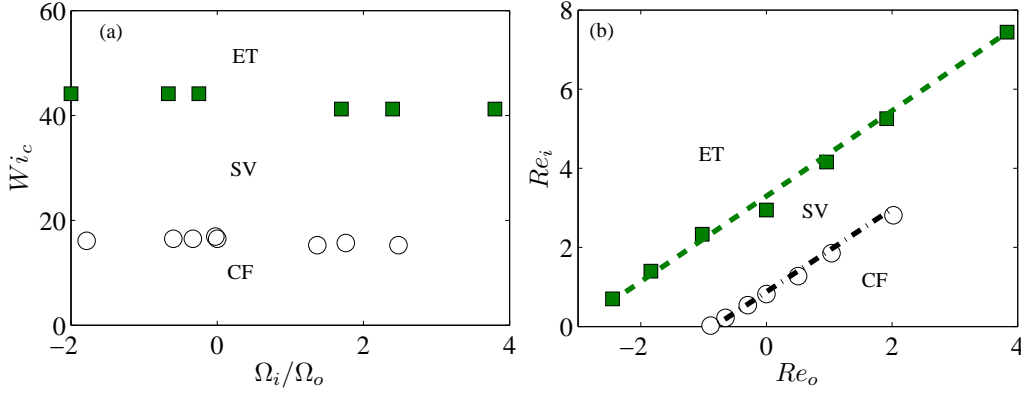


FIG. 8: (a) Critical Weissenberg number versus rotation ratios for different transitions at  $T = 22^\circ\text{C}$ . (b) Critical Reynolds number at the inner cylinder versus Reynolds number at the outer cylinder for the CF (Couette flow) to SV (Stationary vortices) and ET (elastic turbulence) transitions at  $T = 22^\circ\text{C}$ .

At high elasticity ( $El \gg 1$ ,  $T = 22^\circ\text{C}$ ), where the surfactant solution exhibits shear banding, the instability is purely elastic. Fardin et al. [33], considering the case of a stationary outer cylinder, showed that the critical threshold for the onset of instability is set by the Weissenberg in the high shear band for their system. We explore a wide range of rotation ratios and report a constant Weissenberg number for onset of instability, further supporting the idea that the instability is purely elastic. Negative rotation ratios refer to counter rotation whereas, positive ratios denote co-rotation of the cylinders. Fig. 8(a) shows the critical Weissenberg numbers for the onset of stationary elastic vortices and elastic turbulence are constant and about  $Wi_c \approx 15.8 \pm 1$  and  $Wi_c \approx 42.8 \pm 2$ , respectively. Fig. 8(b) indicates the critical Reynolds number associated with the two transitions reported for shear banding wormlike micelles. Fig. 8(b) shows that the critical  $Re_i$  increases with increasing  $Re_o$  such that the instability always starts at a fixed critical shear rate

(or Weissenberg number). We also calculated the slopes of the critical curves in Fig. 8(b) for the two transitions. For transition from CF to SV the slope is  $\approx 0.97$  whereas for SV to ET transition the magnitude of slope is  $\approx 1.05$ .

At moderate elasticity ( $El \approx 1$ ), the viscoelastic surfactant solution no longer exhibits shear banding and is still highly shear thinning. In this range, we expect both inertia and elasticity to play a substantial role in instabilities and transitions. Fig. 9(a) shows the critical Weissenberg number for the onset of instabilities versus the rotation ratio. For  $\Omega_i/\Omega_o = 0$ , (i.e., a stationary inner cylinder), the Weissenberg number for the first transition shows a maximum ( $Wi_c \approx 26.2$ ) and at high rotation ratios (either positive or negative) the critical Weissenberg number approaches an asymptotic value ( $Wi_c \approx 12.2$ , roughly consistent with the value reported above when  $\Omega_o = 0$ , and  $|\Omega_i/\Omega_o| \rightarrow \infty$ ). Recalling that for a Newtonian fluid, the flow is stable when only the outer cylinder is rotated until a catastrophic transition to turbulence at  $Re_o$  of order 40,000 [44], we expect that for  $\Omega_i/\Omega_o = 0$ , and the conditions considered here, inertial destabilization plays no role and therefore, the flow will become unstable via a purely elastic mechanism. Thus, the threshold of instability should be set by a critical Weissenberg number. This critical Weissenberg number ( $Wi \approx 26.2$ ) is somewhat higher than the value reported for onset of the purely elastic instability at  $El \gg 1$ , possibly reflecting stabilization of the flow by the higher solvent contribution to the viscosity ratio. As the inner cylinder rotation increases from zero, either via co- or counter-rotation, the effects of inertia are apparent in the rapid decrease in the critical  $Wi$  to  $Wi \approx 12.2$  for  $|\Omega_i/\Omega_o| \approx 5$ . Fig. 9(b) also shows the critical  $Re_i$  versus  $Re_o$  for the two transitions

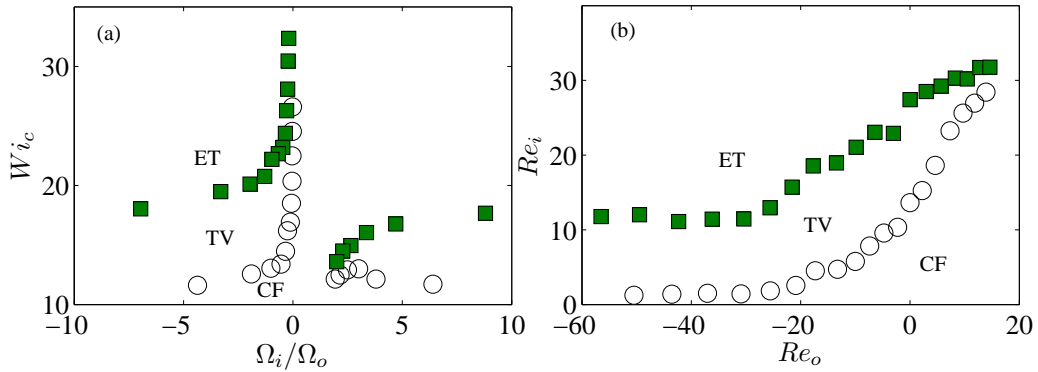


FIG. 9: (a) Critical Weissenberg number versus rotation ratios for transition from CF (Couette flow) to TV (traveling vortices) at  $El \approx 0.97$  and for TV to ET (elastic turbulence) at  $El \approx 0.72$  and  $T = 26^\circ\text{C}$ . (b) Reynolds number at the inner cylinder versus Reynolds at the outer cylinder for different transitions at  $T = 26^\circ\text{C}$ .

for  $El \approx 1$ . First, we note that the critical  $Re_i$  for the first transition, for all  $Re_o$  probed, is a small fraction of  $Re_i$  for the Newtonian case (where  $Re_i \approx 140$  at  $Re_o = 0$ ). In addition, the first transition at  $El \approx 0.97$  is to the travelling wave structures identified above (cf. Fig. 4(a))

rather than to Taylor vortex flow (as reported by Dutcher and Muller [13] for all  $El \leq 0.023$ ) or stationary vortices (reported by Dutcher and Muller [21] for  $El \approx 0.1 - 0.2$ ). The critical Reynolds number at the inner cylinder for onset of travelling vortices decreases as we rotate the cylinders in counter rotation fashion and finally approaches an asymptotic value of  $Re_i \approx 1.38$  for  $Re_o < -25$ .

At low elasticity ( $El \approx 0.034$ ), inertial destabilization becomes more dominant, but transitions are still affected by the elasticity of the fluid. Therefore, we expect the Reynolds number to be more relevant than a Weissenberg number in this range of elasticity. Fig. 10(a) shows that the critical Weissenberg number for instability thresholds is smaller than the ones reported in Fig. 9(a), but the two figures show similar trends with respect to the rotation ratio. Counter-rotation of the outer cylinder reduces the Reynolds number for the onset of instability and gives rise to a minimum value near  $Re_o \approx -54$ . As  $Re_o$  is decreased beyond this value, the instability thresholds increase and at  $Re_o \approx -170$ , the RSW state completely disappears and Couette flow transitions directly to disordered oscillations. A similar trend was also reported for polymeric solutions at low elasticity by Dutcher and Muller [13].

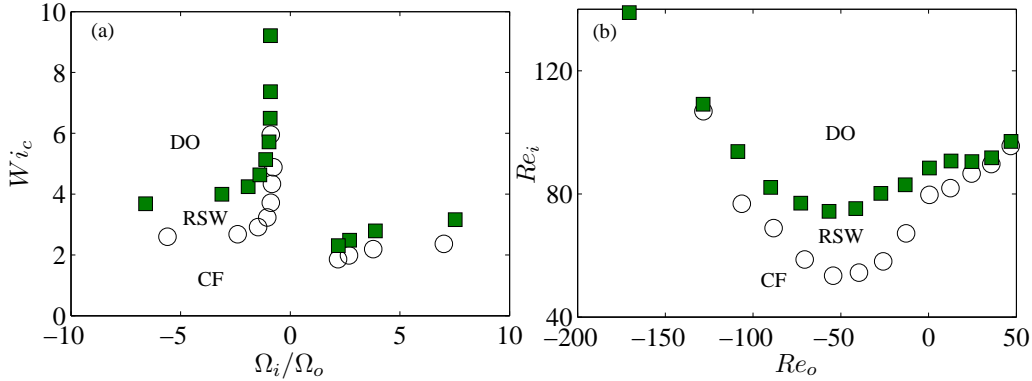


FIG. 10: (a) Critical Weissenberg number versus rotation ratios for transitions CF (Couette flow), RSW (rotating standing waves) and DO (disordered oscillations) for  $El \approx 0.04$  at  $T = 30^\circ\text{C}$ . (b) Reynolds number at the inner cylinder versus Reynolds at the outer cylinder for different transitions at  $T = 30^\circ\text{C}$ .

#### IV. CONCLUSION

In this work, we studied rheological and flow transitions in a model wormlike micelle solution based on CTAB/NaSal over a wide range of elasticity. The main experimental findings can be summarized as below:

At low temperatures (e.g.  $T = 22^\circ\text{C}$  and  $T = 24^\circ\text{C}$ ), wormlike micelle solutions exhibit shear banding in rheological measurements and in Taylor-Couette flow show the formation of stationary

elastic vortices beyond a critical condition,  $K_C \approx 3$  followed by elastically dominated turbulence as the flow strength is increased. The first transition is characterized by an asymptotic wavelength which turns out to be higher than the dimensionless wavelength reported for the shear banding wormlike micelle system CTAB/NaNO<sub>3</sub> at the onset of instability. One possibility is that the differences in critical threshold for onset of instability in the shear banding fluid of CTAB/NaSal ( $K_c \approx 3$ ) and CTAB/NaNO<sub>3</sub> ( $K_c \approx 1$ ) might potentially stem from wall slip at the inner cylinder. Unfortunately, the turbidity contrast for this wormlike micellar solution is not high enough to visualize the  $r - z$  plane of the Taylor-Couette cell and measurements of wall slip are beyond the scope of the present study. With regard to the difference in wavelength between the two wormlike micellar systems, we note that both experiments and theory for linear polymer solutions indicate that wavelength is sensitive to the details of the shear thinning [7]. Moreover, the shear banding wormlike micellar solution did not show any sign of hysteresis. Rotation of both inner and outer cylinder yielded a similar elastic instability that is characterized by a constant Weissenberg number under these high elasticity conditions.

In the intermediate range of temperature, where surfactant solutions are viscoelastic and shear thinning, Taylor-Couette experiments revealed a range of flow transitions and instabilities. Starting with  $T = 26^\circ\text{C}$ , at a moderate elasticity  $El \approx 1$ , we report a first transition from Couette flow to the formation of vortices that are no longer stationary and typically originate at the middle of the cylinders and move towards both the bottom and the top of the cylinders. To the best of our knowledge, this is a new transition for viscoelastic surfactant solutions. These travelling waves are followed by a regime akin to elastic turbulence. At this temperature, rotation of the cylinders in counter fashion lowers the critical threshold for the onset of the travelling wave transition until  $Re_i$  reaches an asymptotic value of  $Re_i \approx 1.38$  for  $Re_o < -25$ . Increasing the temperature to  $T = 28^\circ\text{C}$  reduces the viscosity and a transition from Couette flow to disordered oscillation is reported at elasticity of  $El \approx 0.2$ . At  $T = 30^\circ\text{C}$  and  $El \approx 0.034$ , a transition from Couette flow to rotating standing waves and disordered oscillations is observed. Finally, at  $T = 32^\circ\text{C}$ , the surfactant solution is slightly shear thinning and a transition from Couette flow to TVF  $\rightarrow$  RSW  $\rightarrow$  DO is observed. Most of the instabilities in this range of elasticity are supercritical and show no hysteresis except for  $T = 28^\circ\text{C}$  and  $T = 30^\circ\text{C}$  for which disordered oscillations are replaced by solitary vortex pairs as  $Re_i$  decreases.

At the highest temperature ( $T = 35^\circ\text{C}$ ), rheological measurements indicate nearly Newtonian behavior, and flow visualization experiments in the Taylor-Couette cell also reveal Newtonian transitions. Rotation of both cylinders shifts the thresholds for onset of instability akin to results reported for weakly elastic polymer solutions.

Finally, we note that some of our results on this surfactant solution are different from observations

made on other wormlike micelle solutions or polymer solutions. These differences may arise from a number of factors including different range of viscosity ratios, different extent of shear thinning, different breakage times (in case of wormlike micelle solutions), different extensional behaviors, differences in the wall slip, and differences in the ramping protocols. In table (II), we summarize the transitions observed in the literature and in the present work for both polymer solutions and wormlike micelle solutions. As indicated in table II, the range of viscosity ratio reported in this paper (23 - 1340) is much higher than those tested for polymer solutions (0 - 12.4). Other rheological differences between solutions, e.g. differences in the breakage time for wormlike micelle solutions, wall slip, and differences in extensional behavior, are harder to measure or find data in the literature. There are, at a minimum, qualitative differences between the CTAB/NaSal system and the CTAB/NaNO<sub>3</sub> system even in the small amplitude oscillatory shear rheology. This is evidenced by a different relaxation mechanism observed for the surfactant solution based on CTAB/NaSal studied in this work that follows a two-mode Maxwell model. The structural characterization of this surfactant solution is beyond the scope of the present work. Future work involves a through characterization of the structure and extensional behavior of these systems, and a better understanding of the origins of the differences in flow behavior between wormlike micellar systems.

Solution	$\eta_p/\eta_s$	$El$	Transition Sequence (increasing $Re = \uparrow$ ) (decreasing $Re = \downarrow$ )	$Re_o$	$R_i/R_o$	$\frac{h}{(R_o - R_i)}$	Ref.
PAAm/ saccharose- water	0.08	0.1-0.15	<u>AZI<math>\uparrow</math>TVF<math>\uparrow</math>RSW<math>\uparrow</math>DO</u>	0	0.708	54	[15]
		0.15-0.22	<u>AZI<math>\uparrow</math>TVF<math>\uparrow</math>DO</u>				
		0.22-0.34	<u>AZI<math>\uparrow</math>DO;</u>				
	0.78	0.023-0.033	<u>DO<math>\downarrow</math>OS<math>\downarrow</math>DW<math>\downarrow</math>AZI</u>		0.708	54	[20]
		0.025	<u>AZI<math>\uparrow</math>RSW<math>\uparrow</math>DO</u>				
	0.82	0.03-0.08	<u>AZI<math>\uparrow</math>TVF<math>\uparrow</math>WVF</u>		0.829	74	[16, 19]
		0.09-0.15	<u>AZI<math>\uparrow</math>TVF<math>\uparrow</math>RSW<math>\uparrow</math>DO</u>				
		0.2-27	<u>AZI<math>\uparrow</math>DO</u>				
PEO/ water	0 - 3.45	0.1-0.15	<u>AZI<math>\uparrow</math>TVF<math>\uparrow</math>WVF</u>	0	0.883	47	[12]
	5.32 - 12.4	0.15-0.22	<u>AZI<math>\uparrow</math>RSW</u>				



PEO/ glycerol- water	<u>0.3</u>	<u>0.00047</u>	AZI↑TVF↑WVF↑MVF↑TTV	0	0.912	60.7	[13]
			AZI↑TVF↑WVF	-100–100			
			AZI↑TVF↑WVF(h)	200–500			
			AZI↑TVF↑WVF↑MVF↑WVF	0			
	<u>0.93</u>	<u>0.0017</u>	MWV↑CWV↑WTV↑MT	0			
			AZI↑TVF↑WVF	-100–100			
			AZI↑TVF↑WVF(h)	200			
			AZI↑TVF↑WVF↑MVF	0			
	<u>0.92</u>	<u>0.0054</u>	↑WVF↑WTV(El)/CWV(El)	-100–0			
			AZI↑TVF↑WVF	200–400			
			AZI↑TVF↑WVF(h)	0			
			AZI↑TVF↑WVF↑MVF↑WVF	-100–100			
	<u>0.78</u>	<u>0.023</u>	AZI↑TVF↑WVF	140–200			
			AZI↑TVF↑WVF(h)	0			
			AZI↑SV↑DRSW↑EDT	-100–150			
			EDT↓DRSW↓RSW↓AZI	-180– -100			
	2.82	~0.1-0.2	AZI↑SV↑DRSW↑EDT	-225			
			EDT↓DRSW↓RSW↓AZI				
			AZI↑DRSW↑EDT				
			AZI↑EDT				
CTAB/NaNO <sub>3</sub>	40 - 50	~0.8-1.1	AZI↑SV↑DRSW↑ET	0	0.92	30	[36]
			ET↓DRSW↓SV↓AZI				
CTAB/NaNO <sub>3</sub>	> 10 <sup>3</sup>	> 10 <sup>3</sup>	AZI↑ZZ↑AF↑SV↑F↑ET	0	0.83-0.96	16-40	[34]
			AZI↑MAF↑MF↑ET		0.53	3.42	
CPCl/NaSal- NaCl	> 10 <sup>3</sup>	6 × 10 <sup>3</sup> –2 × 10 <sup>4</sup>	AZI↑SV↑ET	0	0.92	35.4	[33]
CTAB/NaNO <sub>3</sub>	2.2 × 10 <sup>3</sup> –1.9 × 10 <sup>4</sup>	8.5-73.5	AZI↑SV↑ET	0	0.912	60.7	[26]
CTAB/NaSal	<u>400-1340</u>	<u>3.3-18.6</u>	AZI↑SV↑ET	0	0.912	60.7	This work
			AZI↑SV↑ET	-1–2			
	<u>270-380</u>	<u>0.72-0.99</u>	AZI↑TV↑ET	0			
			AZI↑TV↑ET	-50–20			
	<u>130</u>	<u>0.2</u>	AZI↑DO	0			
			DO↓OS↓DW↓AZI	0			
	<u>70</u>	<u>0.034</u>	AZI↑RSW↑DO	-140–50			
			AZI↑RSW↑DO	< -140			
	<u>39</u>	<u>0.01</u>	AZI↑DO	0			
	<u>23</u>	<u>0.003</u>	AZI↑RSW↑DO	0			
			AZI↑TVF↑WVF↑MWVF	0			

---

TABLE II: Comparison of transition sequences in Taylor-Couette flows of linear flexible polymer solutions and wormlike micelle solutions. The flow state ZZ, AF, F, MAF and MF denote zig-zag, anti-flame, flame, modified anti-flame and modified flame states for wormlike micelle solutions.

## V. SUPPLEMENTARY MATERIAL

See supplementary material for experiments that show more detailed information on CTAB/NaSal and CTAB/NaNO<sub>3</sub> systems.

## VI. ACKNOWLEDGEMENT

The authors gratefully acknowledge the financial support from ACS-PRF 53143-ND9 and also NSF through grant number CBET 1335653. The authors are also grateful to Malvern Instrument for the loan of the Malvern Gemini rheometer.

- 
- [1] G. I. Taylor. Stability of a viscous liquid contained between two rotating cylinders. *Phil. Trans. Roy. Soc. London A.*, 223:289–343, 1923.
  - [2] C. D. Andereck, C. C. Liu, and H. L. Swinney. Flow regimes in a circular Couette system with independently rotating cylinders. *J. Fluid. Mech.*, 164:155–183, 1986.
  - [3] H. L. Swinney and J. P. Gollub. *Hydrodynamic instabilities and the transition to turbulence*. 2nd edn, Springer-Verlag, 1985.
  - [4] P. Chossat and G. Iooss. *The Couette-Taylor problem*. Springer-Verlag, 1994.
  - [5] M. A. Fardin, C. Perge, and N. Taberlet. The hydrogen atom of fluid dynamics-introduction to the Taylor-Couette flow for soft matter scientists. *Soft Matter*, 10:3523–3535, 2014.
  - [6] R. G. Larson. Instabilities in viscoelastic flows. *Rheol. Acta*, 31:213–263, 1992.
  - [7] R. G. Larson, S. J. Muller, and E. S. G. Shaqfeh. The effect of fluid rheology on the elastic Taylor-Couette instability. *J. Non-Newtonian Fluid Mech.*, 51:195–225, 1994.
  - [8] R. G. Larson, E. S. G. Shaqfeh, and S. J. Muller. A purely elastic instability in Taylor-Couette flow. *J. Fluid. Mech.*, 218:573–600, 1990.
  - [9] S. J. Muller, R. G. Larson, and E. S. G. Shaqfeh. A purely elastic transition in Taylor-Couette flow. *Rheol. Acta*, 28:499–503, 1989.
  - [10] B. M. Baumert and S. J. Muller. Axisymmetric and non-axisymmetric elastic and inertio-elastic instabilities in Taylor-Couette flow. *J. Non-Newtonian Fluid Mech.*, 83:33–69, 1999.
  - [11] J. M. White and S. J. Muller. Viscous heating and the stability of Newtonian and viscoelastic Taylor-Couette flows. *Phys. Rev. Lett.*, 84:5130–5133, 2000.

- [12] O. Crumeyrolle, I. Mutabazi, and M. Grisel. Experimental study of inertio-elastic Couette-Taylor instability modes in dilute and semidilute polymer solutions. *Phys. Fluids*, 14:1681–1688, 2002.
- [13] C. S. Dutcher and S. J. Muller. Effect of weak elasticity on the stability of high Reynolds number co- and counter-rotating Taylor-Couette flows. *J. Rheol.*, 55:1271–1295, 2011.
- [14] C. S. Dutcher and S. J. Muller. Spatio-temporal mode dynamics and higher order transitions in high aspect ratio newtonian Taylor-Couette flows. *J. Fluid. Mech.*, 641:85–113, 2009.
- [15] A. Groisman and V. Steinberg. Couette-Taylor flow in a dilute polymer solution. *Phys. Rev. Lett.*, 77:1480–1483, 1996.
- [16] A. Groisman and V. Steinberg. Elastic vs. inertial instability in a polymer solution flow. *Europhys. Lett.*, 43:1480–1483, 1998.
- [17] A. Groisman and V. Steinberg. Mechanism of elastic instability in Couette flow of polymer solutions: Experiments. *Phys. Fluids.*, 10:12451–2463, 1998.
- [18] A. Groisman and V. Steinberg. Solitary vortex pairs in viscoelastic Couette flow. *Phys. Rev. Lett.*, 78:1460–1463, 1997.
- [19] V. Steinberg and A. Groisman. Elastic versus inertial instability in Couette-Taylor flow of a polymer solution: Review. *Philos. Mag. B*, 78:253–263, 1998.
- [20] A. Groisman. Experiments on the Couette-Taylor flow with dilute polymer solutions. Master’s thesis, Weizmann Institute of Science, 1993.
- [21] C. S. Dutcher and S. J. Muller. Effects of moderate elasticity on the stability of co- and counter-rotating Taylor-Couette flows. *J. Rheol.*, 57:791–812, 2013.
- [22] S. J. Muller. Elastically-influenced instabilities in Taylor-Couette and other flows with curved streamlines: a review. *Korea-Australia Rheology Journal*, 20:117–125, 2008.
- [23] S. Lerouge and J. F. Berret. *Shear-induced Transitions and Instabilities in Surfactant Wormlike Micelles*, chapter Polymer Characterization, pages 1–71. Springer, 2009.
- [24] H. Rehage and H. Hoffmann. Viscoelastic surfactant solutions model systems for rheological research. *Mol. Phys.*, 74:933–973, 1991.
- [25] M. E. Helgeson, P. A. Vasquez, E. W. Kaler, and N. J. Wagner. Rheology and spatially resolved structure of cetyltrimethylammonium bromide wormlike micelles through the shear banding transition. *J. Rheol.*, 53:727, 2009.
- [26] H. Mohammadigoushki and S. J. Muller. A flow visualization and superposition rheology study of shear-banding wormlike micelle solutions. *Soft Matter*, 12:1051–1061, 2016.
- [27] M. E. Helgeson, M. D. Reichert, Y. T. Hu, and N. J. Wagner. Relating shear banding, structure, and phase behavior in wormlike micellar solutions. *Soft Matter*, 5:3858–3869, 2009.
- [28] S. Lerouge, M. A. Fardin, M. Argentina, G. Gregoire, and O. Cardoso. Interface dynamics in shear-banding flow of giant micelles. *Soft Matter*, 4:1808–1819, 2008.
- [29] N. Dubash, P. Cheung, and A. Q. Shen. Elastic instabilities in a microfluidic cross-slot flow of wormlike micellar solutions. *Soft Matter*, 8:5847, 2012.
- [30] S. Haward, T. J. Ober, M. S. N. Oliveira, M. A. Alves, and G. H. McKinley. Extensional rheology and elastic instabilities of a wormlike micellar solution in a microfluidic cross-slot device. *Soft Matter*, 8:536–555, 2012.
- [31] P. Nghe, S. M. Fielding, P. Tabeling, and A. Ajdari. Interfacially driven instability in the microchannel flow of shear-banding fluid. *Phys. Rev. Lett.*, 104:248303, 2010.
- [32] H. Mohammadigoushki and S. J. Muller. Sedimentation of a sphere in wormlike micellar fluids. *J.*

- Rheol.*, 60:587, 2016.
- [33] M. A. Fardin, T. Divoux, M. A. Guedeau-Boudeville, I. Buchet-Maulien, J. Browaeys, G. H. McKinley, S. Manneville, and S. Lerouge. Shear-banding in surfactant wormlike micelles: elastic instabilities and wall slip. *Soft Matter*, 8:2535–2553, 2012.
  - [34] M. A. Fardin, T. J. Ober, V. Grenard, T. Divoux, S. Manneville, G. H. McKinley, and S. Lerouge. Interplay between elastic instabilities and shear-banding: three categories of Taylor-Couette flows and beyond. *Soft Matter*, 8:10072–10089, 2012.
  - [35] S. Lerouge, M. Argentina, and J. P. Decruppe. Interface instability in shear-banding flow. *Phys. Rev. Lett.*, 96:088301, 2006.
  - [36] C. Perge, M. A. Fardin, and S. Manneville. Inertio-elastic instability of non shear-banding wormlike micelles. *Soft Matter*, 10:1450–1454, 2014.
  - [37] Z. Chu, C. A. Dreiss, and Y. Feng. Smart wormlike micelles. *Chem. Soc. Rev.*, 42:7174, 2013.
  - [38] N. Abcha, N. Latrache, F. Dumouchel, and I. Mutabazi. Qualitative relation between reflected light intensity by Kalliroscope flakes and velocity field in the Couette-Taylor flow system. *Exp. Fluids*, 45:85–94, 2008.
  - [39] C. S. Dutcher. *Experimental investigations into the transitions to turbulence in Newtonian and drag-reducing polymeric Taylor-Couette flows*. PhD thesis, University of California, Berkeley., 2009.
  - [40] J. F. Berret, J. Appell, and G. Porte. Linear rheology of entangled wormlike micelles. *Langmuir*, 9:2851–2854, 1993.
  - [41] See supplementary material for experiments that show more detail information on CTAB/NaSal and CTAB/NaNO<sub>3</sub> systems.
  - [42] M. A. Fardin, T. J. Ober, C. Gay, G. Grgoire, G. H. McKinley, and S. Lerouge. Criterion for purely elastic Taylor-Couette instability in the flows of shear-banding fluids. *Europhysics Letters*, 96:44004, 2011.
  - [43] M. A. Fardin and S. Lerouge. Instabilities in wormlike micelle systems. *Eur. Phys. J. E*, 35:91, 2012.
  - [44] D. Coles. Transition in circular Couette flow. *J. Fluid. Mech.*, 21:385–425, 1965.